Front. Energy 2022, 16(1): 49–63
https://doi.org/10.1007/s11708-022-0817-9

REVIEW ARTICLE

Zhi JIANG, Zhen YE, Wenfeng SHANGGUAN

Recent advances of hydrogen production through particulate semiconductor photocatalytic overall water splitting

Abstract Solar energy-driven photocatalytic water splitting has been investigated for decades to produce clean and renewable green hydrogen. In this paper, the cutting-edge research within the overall water splitting system is summarized from the one-step photocatalytic overall water splitting (POWS) system to the two-step system and the cocatalysts research in this field. In addition, the photocatalytic reaction engineering study is also reviewed which is crucial for future scale-up. This mini-review provides a picture of survey of recent progress of relevant overall water splitting system, with particular attention paid to material system and mechanistic breakthroughs, and highlights the challenge and opportunity of the current system.

Keywords photocatalysis, overall water splitting, hydrogen

1 Introduction

Hydrogen is an attractive energy carrier to replace non-renewable fossil fuels in meeting the challenge of growing global energy demand in the context of a sustainable society, due to its high energy capacity and environment-friendly qualifications. The traditional production of hydrogen requires the consumption of hydrocarbon and/or water. In contrast, the direct splitting of water into hydrogen (H_2) and oxygen (O_2) by sunlight in one step is one of the most promising routes to the so-called 'photocatalytic overall water splitting'(POWS), since it does not rely upon fossil fuels and nominally results in zero CO_2 emissions [1]. High efficiency photocatalysts for hydrogen production are thus a key goal for the field of photocatalysis, driven by the desire to achieve artificial photosynthesis and thus produce solar fuels in a scalable and cost-effective way [2].

Electron donors such as methanol, ethanol, lactic acid, and Na_2S/Na_2SO_3 could be used together with water instead of pure water in overall water splitting. Since electron donors are more readily oxidized than water, the remaining electrons subsequently reduce water to produce H_2, whose reaction involves only the evolution of hydrogen [2,3]. Such reaction is a half reaction of POWS reaction, named hydrogen evolution reaction (HER). Although sacrificial reagents are also effective in suppressing undesired recombination processes and thus enhancing the hydrogen evolution, such reaction is typically exergonic ($\Delta G < 0$). Comparatively, water splitting is a highly endergonic reaction with ΔG° = 275 kJ/mol [2–4]. Generally, considering the estimated average cost of the hydrogen produced by the particulate system, only the overall water splitting system is considered. It is estimated that, only when the solar-to-hydrogen conversion efficiency (STH) value of the overall water splitting system reach 10%, could the hydrogen production price be in the range of 1.6–3.5 USD/kg to meet the economical requirement suggested by United States Department of Energy [1,4,5]. Most recently, it was reported that photocatalytic water splitting of the $SrTiO_3$:Al reaches a maximum STH of 0.76% in a 100-m^2 array of panel reactors running over several months [6]. This system demonstrated safety, durability, simplicity, and low cost for system design and maintenance. Therefore, although this STH (0.76%) has still fallen short of the efficiency to reach the commercial purpose, more efficient photocatalytic materials developed in the future could facilitate the practical application of photocatalytic water splitting, one of the ultimate goals for energy researchers.

Over the past decades, heterogeneous photocatalysis has received extensive attention with a vision to efficiently convert solar energy into solar fuels and realize large-scale commercial application such as for environmental

Received Nov. 19, 2021; accepted Dec. 23, 2021; online Mar. 10, 2022

Zhi JIANG (✉), Zhen YE, Wenfeng SHANGGUAN (✉)
Research Center for Combustion and Environment Technology, Shanghai Jiao Tong University, Shanghai 200240, China
E-mail: zhijiang@sjtu.edu.cn (Zhi JIANG);
shangguan@sjtu.edu.cn (Wenfeng SHANGGUAN)

application purpose. Indeed, many excellent reviews spanning the search for new photocatalytic materials or improved synthetic routes already exist [1,2,7–22]. Hence in this paper, several progresses of photocatalytic overall water splitting system in recent years were exclusively focused on. First, the one-step photocatalytic overall water splitting system and cocatalysts were introduced. Then, the two-step photocatalytic overall water splitting system and cocatalyst used in the photocatalytic OWS system were reviewed. Finally, studies on photocatalytic reaction engineering were also introduced, which was also important for scale-up water splitting in the future.

2 Semiconductor photocatalyst in one-step overall water splitting system

Photocatalytic one-step overall water splitting (POWS) means the simultaneous hydrogen as well as oxygen evolution reactions on a single photocatalyst. The key processes in the one-step photocatalytic water splitting reaction include photon absorption by a semiconductor leading to the generation of electron-hole sets; charge separation as well as its migration to the semiconductor surface; and charge transfer and subsequent surface chemical reactions generating H_2 and O_2. Photo-generated charges must possess sufficient thermodynamic driving forces to satisfy the redox potentials necessary for water splitting. This is controlled by the bandgap, as well as the position of the valence and conduction band edges of a photocatalyst. Photocatalysts with desirable band structures capable of generating charges with the requisite energies for water splitting are currently developed by largely empirical band engineering approaches [8–18]. To achieve the photocatalytic overall water splitting, the conduction band bottom of the photocatalyst need to be higher than the reduction potential of water and the valence band top should be lower than the oxidation potential of water. The bandgap energy of the semiconductor should then be higher than the theoretical decomposition potential of water (1.23 V) due to the overpotential, and should generally be above 2 eV, corresponding to a light absorption range below 600 nm.

Generally, the photocatalysts which can split water into stoichiometric H_2 and O_2 in the one-step excitation step could be categorized into photocatalysts which could absorb ultraviolet light excitation (UV) only light ($\lambda <$ 400 nm) or with a bandgap sufficient enough to absorb visible light ($\lambda > 400$ nm).

Up to the present, the major photocatalyst materials reported for POWS are semiconductors which can absorb UV only light ($\lambda < 400$ nm). Such compound could be classified as compounds such as Ti^{4+}, Zr^{4+}, Ta^{5+}, Nb^{5+}, and W^{6+} based materials with electron-free filled state d^0 electron configuration and In^{3+}, Ga^{3+}, Ge^{4+}, Sn^{4+}, and Sb^{5+} based photocatalytic materials with d^{10} electron configuration, i.e., the d-electron orbitals of the metal ions are in the full electron filled state (d^{10}). The conduction band minimum (CBMs) of the bandgap of such metal compounds is generally composed of the d orbitals (d^0 configuration) or sp orbitals (d^{10} configuration). Therefore, such compounds generally have a high (more negative) conduction band position, which is sufficient for the reduction of H_2O to H_2. Comparatively, the valence band maximums (VBMs) for such compound are comprised of O_{2p} orbitals and are located at approximately 3 V (versus NHE, at pH = 0). Therefore, d^0 as well as d^{10}-type oxides generally show an excess potential difference for the OER and HER.

Some alkali metal, alkaline earth metal, or other metal ions can be introduced into the above compounds to form some salts, such as titanates, niobates, tantalates, tungstate, zirconate for d^0 metal ions and indium salts, gallate, germinate, stannate, and antimonates for d^{10} metal ions [1,23]. Salts such as $SrTiO_3$, $CaTiO_3$, $Na_2Ti_6O_{13}$, $K_2Ti_6O_{13}$, $BaTi_4O_9$, $K_2La_2Ti_3O_{10}$, $K_4Nb_6O_{17}$, $Ba_5Nb_4O_{15}$, $NaTaO_3$, $KTaO_3$, $PbWO_4$, $BaZrO_3$, $CaIn_2O_4$, $SrIn_2O_4$, $ZnGa_2O_4$, Zn_2GeO_4, Sr_2SnO_4, and $NaSbO_3$ [1,23] showed a good photocatalytic ability. Among the above catalyst, most recently, the $SrTiO_3$ photocatalyst demonstrates a POWS activity with an internal quantum efficiency (IQE) of 100% at wavelengths between 350 and 360 nm by applying a combination strategy including aliovalent metal cations doping (aluminum) to suppress the Ti^{3+} defect, using flux treatment to suppress the defects in $SrTiO_3$, cocatalyst, and facet engineering to optimize the separation of the photon generated carries and surface reaction [24].

As noted above, the deep VBM levels typically related to the O 2p orbitals of the semiconductors based upon d^0-type or d^{10}-type metal cations always lead to a wide bandgap semiconductor response UV light ($\lambda < 400$ nm). However, the standard spectrum of a sun (AM1.5) can be roughly divided into the ultraviolet light, the visible light, and the infrared light, which account for 5%, 43%, and 52% of the energy respectively. To reach the 10% STH, photocatalysts that could response to long wavelengths of light (e.g., $\lambda > 400$ nm) should be developed. There are several strategies including the anions or cation doping, and solid solution method established to search POWS semiconductor photocatalyst capable of responding to visible light.

Titanium (TiO_2) could only response to UV light ($\lambda < 400$ nm). Since the success extension of absorption of titanium to visible light range ($\lambda < 500$ nm) by treating the TiO_2 in the flow of ammonium to realize nitrogen doping in 2001 [25], tuning the VB of metal oxide photocatalyst using the p orbitals of anions, including N 2p or S 2p, has motivated the successful development of many anions doping visible light metal oxide photocatalyst. (Oxy) nitrides and (Oxy)sulfides are, therefore, considered as promising candidates for visible light response photocatalysts. For example, the light absorption of TaON and

Ta_3N_5 are shifted to above 500 and 600 nm, respectively compared to Ta_2O_5. This is ascribed to the shift of the VBMs of TaON and Ta_3N_5 to more negative potentials due to nitrogen doping. Interestingly, TaON and Ta_3N_5 are able to produce O_2 and H_2, respectively, under visible light in half-reactions. However, the visible light absorption of TaON and Ta_3N_5 does not show the POWS activity. Wang et al. [26] realized the POWS of Ta_3N_5 in 2018. They synthesized Ta_3N_5 by volatilizing potassium-related species during the nitridation procedure of $KTaO_3$. As shown in Fig. 1, scanning transmission electron microscopy (STEM) images with atomic resolution provided unambiguous structural information on the generation of the Ta_3N_5 crystal phase on the $KTaO_3$ (110) surface. Ta_3N_5 nanorods consisting of single crystals devoid of grain boundaries grown on $KTaO_3$ particles could achieve POWS under visible light as well as simulated sunlight irradiation condition when loaded with Rh/Cr_2O_3 co-catalyst. The AQE were 0.22% at 420 nm (±25 nm), and 0.024% at 500 nm (±25 nm).

Metal chalcogenides are also considered as promising visible light POWS photocatalyst candidates considering their narrow bandgap [27]. However, the chalcogen ion in the lattice will certainly be attacked by the photogenerated hole in such reaction, therefore, resulting in the deviation of the portion of generated H_2 and O_2 from the stoichiometric ratio. Wang et al. [28] demonstrated that oxysulfide, $Y_2Ti_2O_5S_2$ with the bandgap at 1.9 eV is more stable against self-oxidation, because the surface S^{2-} ions are stabilized by hybridization of S-3p and O-2p orbitals. Consequently, $Y_2Ti_2O_5S_2$ showed a stable POWS activity in the 20 h reaction by using IrO_2 and Rh/Cr_2O_3 as OEC oxygen evolution co-catalysts (OEC) and hydrogen evolution co-catalysts (HEC), respectively. Such results clearly showed the possibility of anions doping semiconductor to achieve POWS if the crystallinity of the semiconductor and reaction condition could be well controlled.

Doping metal cation ions in the metal oxide is another efficient way to sensitize metal oxide photocatalysts to visible light. For example, as depicted in Fig. 2, $Rh:SrTiO_3$ demonstrated the intrinsic absorption edge at 380 nm corresponding to the bandgap excitation of $SrTiO_3$. The Rh doping lead to the visible light absorption at 580 nm which could be related to the electron transition from the Rh 4d state to the conduction band (Ti 3d orbitals) [29]. Consequently, under visible light irradiation ($\lambda >$ 440 nm), $Rh:SrTiO_3$ could efficiently produce H_2 from water when methanol was used as sacrificial reagent [30]. $Pt/Rh:SrTiO_3$ (Pt, 0.1% (weight fraction)) even demonstrated a quantum yield of 5.2% at 420 nm for H_2 evolution reaction. Kudo et al. [31–33] further suggested to overcome the charge recombination problems in Rh-doped Rh (1%) $SrTiO_3$ by co-doping metal ions. Interestingly, $SrTiO_3$:Rh/Sb, i.e., co-doping $SrTiO_3$ with antimony and rhodium, showed a POWS activity under visible light irradiation (AQY = 0.1%, 420 nm), although the introduced d band by doping was generally believed to be discrete because of the low doping concentration ($< 2\%$ (atom percentage)). It was believed that co-doping Rh with Sb stabilized Rh^{3+} ions and suppressed the generation of Rh^{4+} ions and oxygen vacancies. The latter generally functioned as recombination sites. This successful example indicates that it is feasible to design visible light response metal oxide semiconductor photocatalysts for POWS by doping or co-doping metal ions.

Alloying different bandgap semiconductors into a solid solution is another method to tune the bandgap structure. A landmark work on solid-solution photocatalysts $(Ga_{1-x}Zn_x)$ $(N_{1-x}O_x)$ was reported by Maeda et al. [34,35] in 2005. ZnO and GaN were semiconductors with similar lattice parameters (ZnO: $a = b = 0.325$, $c = 0.521$ nm and GaN: $a = b = 0.319$, $c = 0.519$ nm). GaN and ZnO were also wide-bandgap semiconductors with a bandgap energy of 3.4 and 3.2 eV, respectively. However, it is interesting to note that the bandgap of the solid solutions of GaN and ZnO, i.e., $(Ga_{1-x}Zn_x)$ $(N_{1-x}O_x)$ become narrower at about 2.6 eV as the CBM consists mainly of 4s and 4p orbitals of Ga, while the VBMs consists of N 2p and Zn 3d orbitals. The N 2p and Zn 3d electrons in the higher valence band provide the p-d repulsion with the VBMs, resulting in a narrower bandgap and a red-shifted absorption spectrum. $Rh_{2-y}Cr_yO_3$ (2.5% (weight fraction) Rh, 2% (weight fraction) Cr)/$(Ga_{1-x}Zn_x)(N_{1-x}O_x)$ exhibits an apparent quantum efficiency (AQE) of 5.9% at 420–440 nm [36]. Recently, Pan et al. [37,38] also reported that the following two solid solution, $LaMg_xTa_{1-x}O_{1+3x}N_{2-3x}$ (x = 1/3) solid solution (solid solution of the oxynitride $LaTaON_2$ and the complex oxide $LaMg_{2/3}Ta_{1/3}O_3$) and $LaSc_xTa_{1-x}O_{1+2x}N_{2-2x}$ series ($0 < x < 0.75$) solid solution, showed a POWS activity at the visible light range ($\lambda >$ 600 nm).

In the past decade, Liu et al. [39,40] developed a series of Bi-based solid solution photocatalysts-$Bi_{1-x}M_xVO_4$ (M = Y, Dy, La, Sm, Nd, Gd, Eu) with a POWS activity. Using $Bi_{0.5}Y_{0.5}VO_4$ as an example, DFT calculation reveals that the Y cations not only made an indirect contribution by deteriorating the interactions between Bi and VO_4 tetrahedra but also elevated the CBM of $BiVO_4$. As a result, $Bi_{0.5}Y_{0.5}VO_4$ are capable of absorbing visible light (470 nm) as well as showing a band structure that satisfies the demand of both proton reduction and water oxidation in half reaction (Fig. 3) [40]. However, $Bi_{1-x}M_xVO_4$ (M = Y, Dy, La, Sm, Nd, Gd, Eu) does not show POWS at a wavelength above 420 nm. Inspired by the spatial separation effect of $BiVO_4$ ({010} and {110} crystal facets) proposed by Li et al. [41], $Bi_xY_{1-x}VO_4$ with a dodecahedron shape exposing two different energy facets ({1 0 1} and {1 0 0}), was reported to be synthesized in 2018 [42]. The photogenerated carriers were suggested to be separated between the adjacent exposed facets, which finally was reported to deliver an enhanced POWS activity.

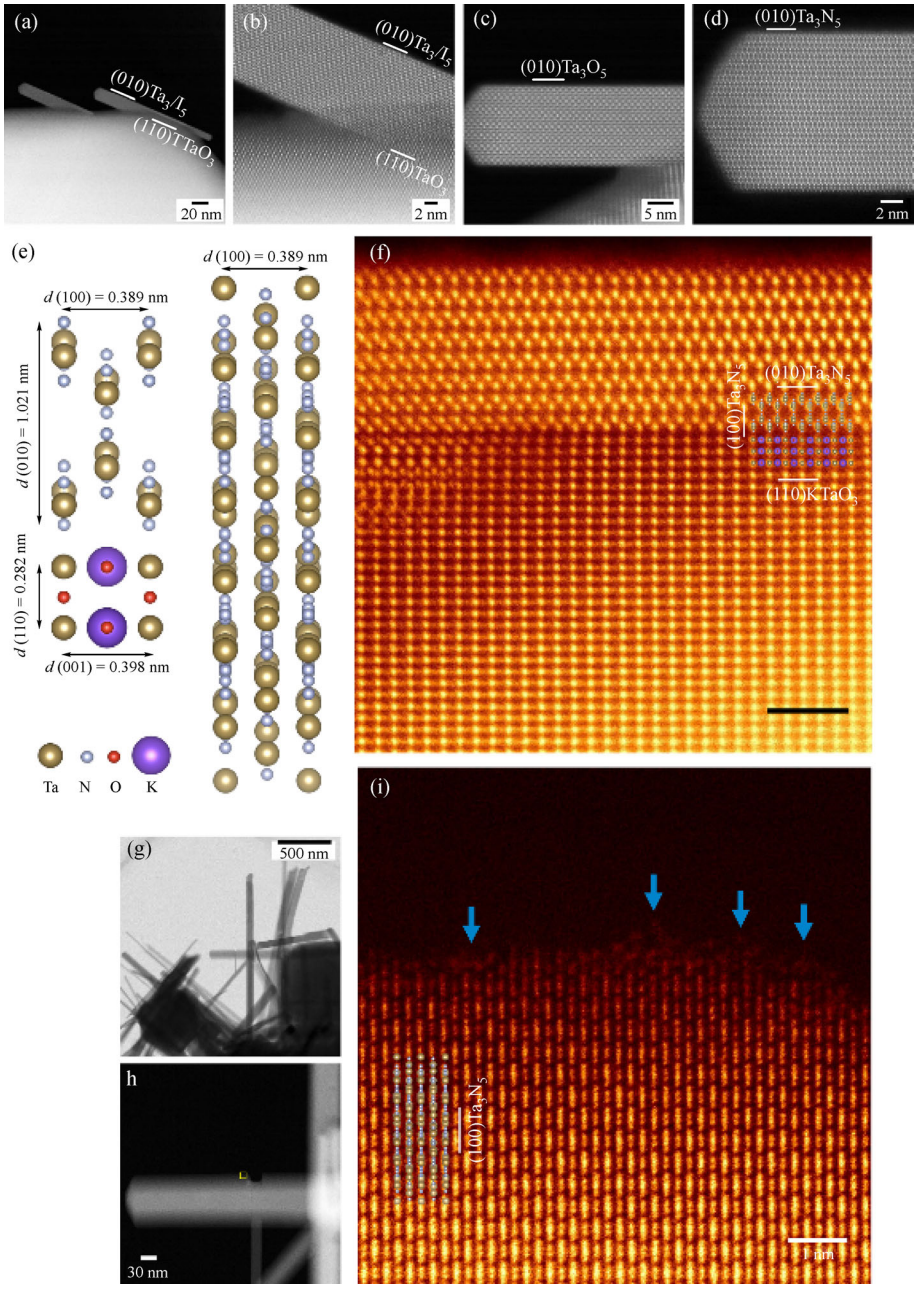

Fig. 1 Single-crystal structure of Ta_3N_5 nanorods grown on $KTaO_3$ (adapted with permission from Ref. [26]).
(a–d) ADF-STEM images of $Ta_3N_5/KTaO_3$ synthesized with a nitridation time of 0.25 h, viewed from the [001] direction of the Ta_3N_5. (The lines indicate the crystal facets); (e) crystal structures of Ta_3N_5 projected from the [001] (top left) and [041] (right) directions, and $KTaO_3$ projected from the direction (bottom left), depicted using the Vesta program. (*d* indicates the interplanar distance); (f) colorized and magnified ADF-STEM images of a Ta_3N_5 nanorod in $Ta_3N_5/KTaO_3$ synthesized with a nitridation time of 0.25 h viewed from the [001] direction of the Ta_3N_5. Insets: depicted crystal structures of Ta_3N_5 projected from the [001] direction and $KTaO_3$, as shown in (e). (The lines indicate the crystal facets) (g–h) ADF-STEM images of $Ta_3N_5/KTaO_3$ synthesized with a nitridation time of 4 h; (i) colorized and magnified ADF-STEM images of a Ta_3N_5 nanorod in $Ta_3N_5/KTaO_3$ synthesized with a nitridation time of 4 h, viewed from the [041] direction of Ta_3N_5 and corresponding to the square area in (h). Inset: depicted crystal structure of Ta_3N_5 projected from the [041] direction, as shown in (e). The arrows and the line indicate the disordered atom arrangement at the surface and the crystal facet, respectively.

Polymer carbon nitride (PCN) is another group different from the above mentioned materials as it is a metal-free photocatalyst [43]. Wang et al. reported PCN with a bandgap at about 2.8 eV related with the absorption edge at about 442 nm could produce hydrogen under sacrificial conditions in 2008 [43]. Theoretical calculations indicate that the VBM and CBM of this PCN primarily were comprised by N 2pz and C 2pz orbitals, respectively. By using proper cocatalyst, i.e., Pt, PtO_x, and CoO_x, Zhang et al. [44] revealed that POWS could also be realized by

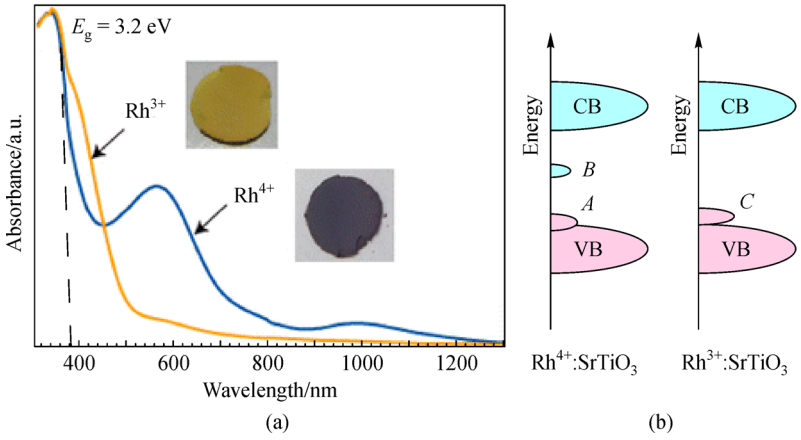

Fig. 2 Bandgap structure of Rh:$SrTiO_3$ (adapted with permission from Ref. [29]).
(a) Absorption spectra; (b) scheme of the electronic structures of Rh:$SrTiO_3$.

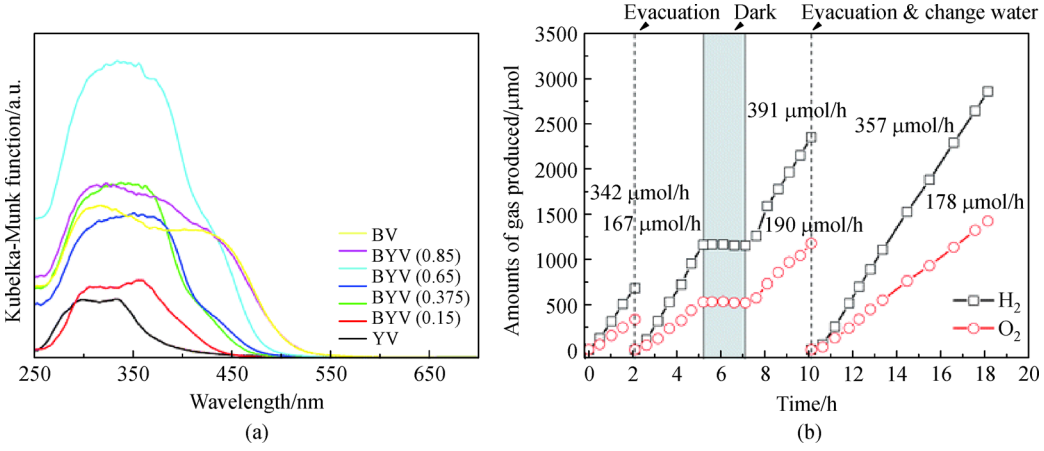

Fig. 3 (a) Absorption spectra of the $Bi_xY_{1-x}VO_4$ and (b) POWS activity over BYV(0.375) ($\lambda > 300$ nm) (adapted with permission from Ref. [40]).

using PCN in 2016. Such combination finally delivered a POWS activity with an AQY of 0.3% at 405 nm. Recently, by using highly crystalline polythiazide imides (PTI) intercalated with LiCl (PTI/Li^+Cl^-) as a model conjugated polymer photocatalyst, Lin et al. [45] further revealed that increasing the portion of reactive facets could considerably improve the POWS efficiency of PTI/Li^+Cl^-, which finally delivered an AQY of 8% at 365 nm. Most recently, Liu et al. [46] reported a fully condensed poly (triazine imide) crystal with extended π-conjugation and deficient structural defects could efficiently drive the one-step POWS with a recorded AQE of 12% at 365 nm.

In recent years, covalent organic frameworks (COFs) and metal-organic frameworks (MOFs) materials have attracted extensive research interest in photocatalysis study [47,48]. COFs and MOFs exhibit structural advantage such as a well-defined and tailorable structure which generally composes of periodic units [47–49]. Recently, a high crystalline and hydrophilic triazine-based COF (CTF-HUST-A1) displayed a POWS activity when 4.5% (weight fraction) of NiP_x and 3.0% (weight fraction) of Pt was loaded as co-catalysts [50]. Such success suggests that although it is still challenging, there is a great potential in developing such material in the POWS area.

3 Two-step photocatalytic overall water splitting system

The Z-scheme photocatalysis system is a two-step system inspired by the photosystem II-photosystem I (PSII/PSI) in natural photosynthesis [51]. Generally, the Z-scheme is composed of a hydrogen-evolution photocatalyst, an oxygen-evolution photocatalyst, and an electron mediator. The advantage of such system lies in the fact that photocatalyst which is only active for hydrogen evolution half reaction or oxygen evolution could be combined in such a system for overall water splitting reaction. However, the efficient transfer of electrons between hydrogen evolution photocatalyst and oxygen evolution

photocatalyst particles is still challenging. In 2016, Wang et al. [52] illustrated that an all-solid-state Z-scheme is capable of splitting water by using a gold layer as the photo-generated carrier layer. As manifested in Fig. 4, SEM images illustrate direct visualization of the hybrid photocatalyst $SrTiO_3$:La,Rh|Au|RuO_2-$BiVO_4$:Mo, which is comprised of $SrTiO_3$:La,Rh as well as $BiVO_4$:Mo particles embedded into a gold layer. This all-solid state Z-scheme hybrid photocatalyst displayed an AQY of 33% at 419 nm as well as an STH of 1.1% in POWS (pH 6.8).

In 2021, Zhao et al. [53] showed an all-solid-state Z-scheme system for POWS. The two-oxygen evolution and hydrogen evolution photocatalyst was both boron-doped carbon nitride. This carbon nitride Z-scheme heterostructure without the transfer layer showed an STH efficiency of 1.16% under one-sun illumination using platinum and Co$(OH)_2$ as co-catalysts. The high POWS efficiency is ascribed to the ultrathin structures, strong interfacial interaction, and staggered band positioning. Chen et al. in 2021 showed another novel all-solid-state Z-scheme system, composed by graphitic carbon nitride/rGO/perylene diimide polymer (g-C_3N_4/rGO/PDIP). This system could realize high-flux charge transfer by a built-in giant internal electric field in the Z-scheme junction which could boost the charge separation efficiency. Therefore, this g-C_3N_4/rGO/PDIP achieved efficient photocatalytic overall water splitting with a notable quantum efficiency of 4.94% at 420 nm and a solar-to-hydrogen energy-conversion efficiency of 0.30% [54].

Zhao et al. [55] proposed another system inspired by the natural photosynthesis, named as hydrogen farm project (HFP). The HFP is consisted of two sub-parts (Fig. 5). One is the photocatalytic water oxidation part. In this sub-system, the photocatalytic reaction takes place to oxidize water to oxygen and reduce the shuttle ions to a reduced state. The shuttle ions were then pumped to another separate sub-part consisted of the electrolysis cell. The ions were oxidized and produced hydrogen in the electrolysis cell. The HFP has the advantages of avoiding gas separation system as the two sub-parts were separated physically. The AQE for photocatalytic oxygen evolution was over 71% in the presence of Fe^{3+} by applying $BiVO_4$ as oxygen evolution photocatalyst with fine-tuned {110} {010} facets. The overall STH efficiency was 1.8% for this system.

4 Cocatalyst

The photoconversion efficiency, on the other hand, mainly depends upon the degree of charge separation and migration in the semiconductor, as well as the kinetics of the surface chemical reactions. Transition metal and metal oxide have been deposited on the surface of semiconductor particles as co-catalysts to improve the photoconversion efficiency of overall water splitting reaction [7–18,56–58].

One of the most typical cocatalyst in photocatalyst study is platinum (Pt). The Pt/TiO_2 powder suspensions in water were shown to be capable of performing heterogeneous photocatalytic water splitting [59], and can be regarded as a model of a short-circuited or miniaturized photoelectrochemical microcell [60], with Pt nanoparticles deposited on the TiO_2 surface as a prototypical co-catalyst. Pt is one of the most commonly studied cocatalyst in the metal-photocatalyst system. This could be ascribed to its own catalytic activity (the overpotential of Pt is the lowest for hydrogen generation among different electrode materials) and its highest work function among such noble metals as Pt(5.65 eV), Pd(5.55 eV), Ni (5.15 eV), Au(5.10 eV), Rh (4.98 eV), Ru(4.71 eV), and Ag (4.0 eV) [61,62]. The

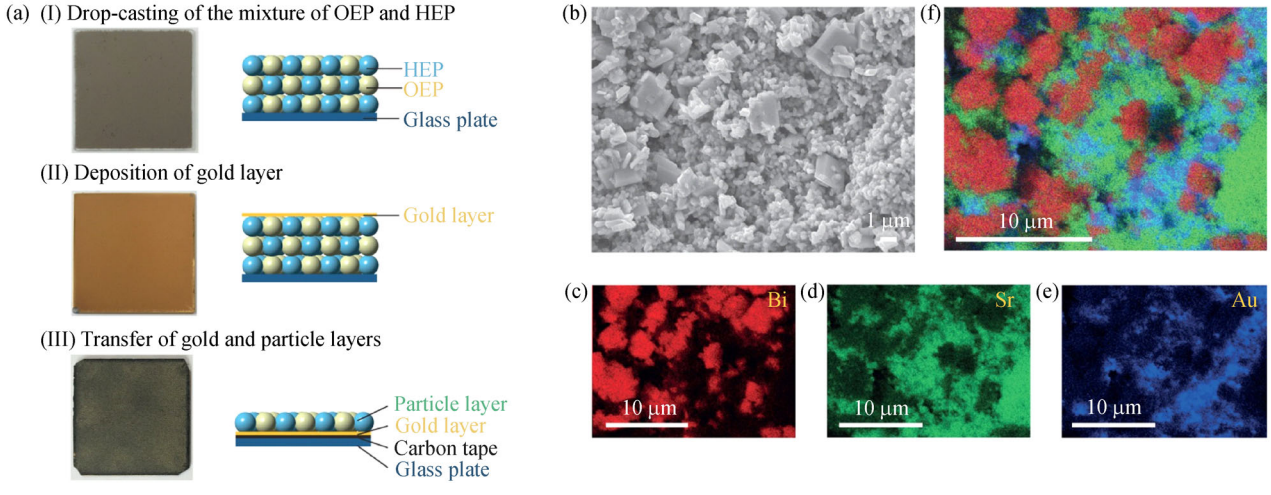

Fig. 4 (a) Illustration of the preparation of the $SrTiO_3$: La, Rh/Au/BiVO4:Mo sheet by the particle transfer method; (b) top-view SEM–EDX elemental mapping images showing an SEM image; (c) Bi distribution; (d) Sr distribution; (e) Au distribution; (f) a superimposition of the distributions (Adapted with permission from Ref.[52]).

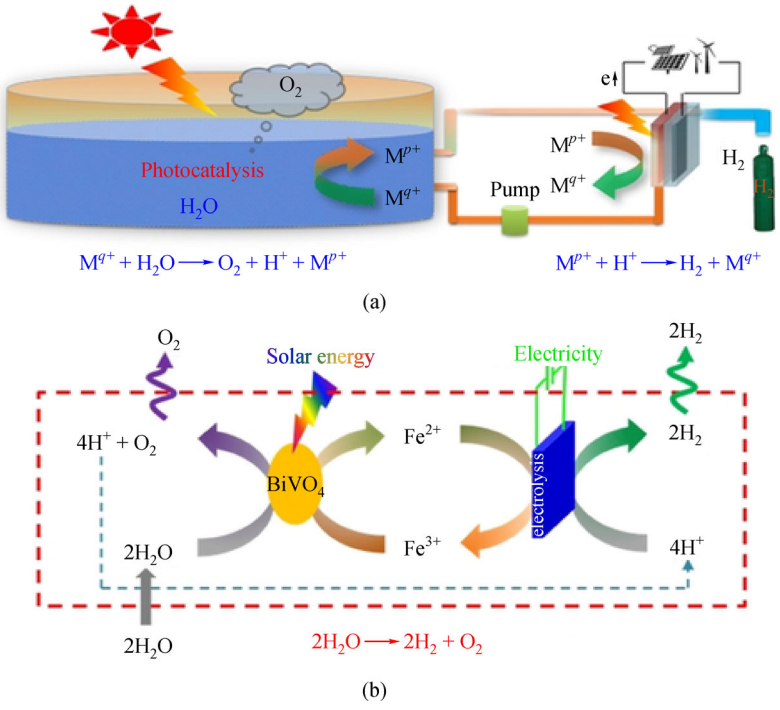

Fig. 5 Scheme of HFP (adapted with permission from Ref. [55]).
(a) The hydrogen farm project (HFP) for scalable solar hydrogen production using particulate photocatalyst for water oxidation and a shuttle ion loop for energy storage; (b) The practical realization for HFP by using $BiVO_4$ as water oxidation photocatalyst, Fe^{3+}/Fe^{2+} as shuttle ions for energy storage, and an electrolysis cell for hydrogen production.

work function of Pt is also higher than TiO_2. The contact of Pt with TiO_2 will lead to the electron migration from TiO_2 to Pt until a thermodynamic equilibrium is reached [9,63]. The bands of the semiconductor bend upward toward the surface, and a Schottky barrier is formed at the interface of Pt and TiO_2 with a barrier height [9].

The dispersion of cocatalyst was one important issue in cocatalysts study. For example, it is found that hydrogen production scales with the interfacial contact area between titania and Pt metal in hydrogen production half reaction using Pt/TiO_2 as photocatalyst [64]. This corresponds with the overall water splitting case using GaN:ZnO modified with different-sized Rh/Cr_2O_3 (core/shell) NPs [65]. It is further found that the interfacial contact area between titania and Pt metal could be characterized by the following parameters, i.e., the Pt metal content divided by the Ti content on the Pt/TiO_2 catalyst surface. This relationship offers a simple spectroscopic method to quantitatively predict the photocatalytic HER performance. An *in situ* polyol-process was, therefore, developed to control the synthesis size and shape of selected platinum nanocrystals on TiO_2. Highly dispersed Pt nanocrystal with different shapes (nanocubes or nanopolyhedra) in the size ranging from 2 nm to 8 nm could be systemically *in situ* grown on the surface of TiO_2 powders [66]. This strategy was demonstrated as an effective method to prepare model hybrid cocatalyst/semiconductor nanocomposite to obtain the sub-10 nm to 1 nm scale insight into the photocatalytic system. Self-photo-degradation was found to be able to efficiently remove the ligands used in the synthesis procedure without affecting the morphology and electron state of the hybrid photocatalyst [67]. The modified *in situ* polyol method was designed to further improve the activity of this system [68], based on the understanding of the growth behavior of platinum on TiO_2 surface in the calcination process [69] and the *in situ* polyol process [67,70].

Recently, Wang et al. [71] also revealed that a sequential decoration of Pt cocatalyst by impregnation-reduction followed by site-selective photo-deposition could increase the H_2 evolution of Pt-loaded $BaTaO_2N$ photocatalyst over 100 times more efficiently than before. The specially designed process was suggested to enable uniform dispersion and intimate contact of cocatalyst nanoparticles on single-crystalline narrow-bandgap particulate photocatalysts. The above studies showed the potential to improve the efficiency of the system based on the understanding of not only the relationship between the structure-performance but also the synthesis-structure of the material.

The chemical state of cocatalyst is another crucial parameter significantly influencing its performance. For example, although Pt is an effective electrocatalytic oxygen reduction reaction (ORR) and is not considered

so suitable for use during the overall water splitting reaction, it is still applied in the overall water splitting photocatalytic study in some cases [71,72]. Recently, Qureshi et al. [72] revealed the insensitivity of ultrafine PtO_x to interact with gases such as H_2, O_2, and CO. Consequently, $SrTiO_3$ decorated with such PtO_x showed an efficient POWS activity.

Nickel (Ni) is another representative chemical-state-effect example in this field. NiO_x was applied as cocatalyst with $SrTiO_3$ in the early 1980s [73]. The chemical state of the loaded Ni strongly influenced the photocatalytic water splitting activity for $NiO_x/SrTiO_3$. Domen et al. [74] demonstrated that the R733-O473 treatment procedure, i.e., a reduction by H_2 and a reoxidation by O_2 at 733 K and 473 K respectively was necessary before using the $NiO_x/SrTiO_3$ photocatalyst. $SrTiO_3$ was not active if no cocatalyst was loaded. $NiO/SrTiO_3$ showed a low activity and the amount of evolved O_2 was less than the stoichiometric amount of H_2. When NiO-loaded $SrTiO_3$ was treated by the R733-O473 procedure, the inner sphere of the loaded NiO was reduced to the Ni metal after H_2 reduction, and successive reoxidation under a mild condition only oxidized the external surface of Ni metal particles. This R733-O473 treatment finally gave a Ni/NiO (core/shell) structure. The $NiO_x/SrTiO_3$ (R733-O473) catalyst is capable of overall water splitting to produce H_2 and O_2 in stoichiometric amount. The NiO layer on Ni was suggested to be capable of suppressing the backward reaction, i.e., the reaction between hydrogen and oxygen to form water, on Ni. The shell NiO could also help suppress the oxidation of the core Ni by water. This Ni core/shell strategy was also an effective chemical-state strategy for other semiconductor photocatalysts besides $SrTiO_3$. For example, a well-dispersed Ni/NiO_x on $K_4Ce_2Ta_{10}O_{30}$ was reported, a solid solution capable of responding to visible light at 540–690 nm, to be 4 times more efficient than another strategy, loading dual cocatalyst Pt and RuO_2 for reduction and oxidation half reactions, respectively [62].

The core/shell structure of NiO/Ni was the first core/shell structure cocatalyst reported in this field [74]. In 2006, Maeda et al. [75] reported a type of core/shell cocatalyst, a noble-metal Rh/Cr_2O_3(core/shell) nanoparticle, which is now the so-called surface nanolayer coating strategy [4]. The core/shell structure (Cr_2O_3 shell at thickness about 2 nm) was proved by XAFS and TEM, and the *in situ* spectroscopic method was applied to investigate the mechanism of H_2 evolution on core/shell-structured nanoparticles [76]. The underlying mechanism suggested that the protons and H_2 molecules could penetrate the Cr_2O_3 layer [11]. However, O_2 was not permeable. This means that the backward reaction of water splitting catalyzed by Rh, i.e., re-oxidization of H_2 was suppressed by the core/shell structure of the cocatalyst. This deposition strategy also worked when using Cr_2O_3 shells on other noble metal or metal oxide cores, such as Pt, Pd, NiO_x, RuO_2, and Rh_2O_3. Other metal oxy(hydroxides) thin shells, such as Ti, Ta, Al, or Nb oxy(hydroxides) could also be applied as selective membrane as the role of Cr_2O_3 [77–82].

The cocatalyst optimized strategy could also be achieved in combination with the dual cocatalyst strategy. For example, Maeda decorate ($Ga_{1-x}Zn_x$) ($N_{1-x}O_x$) using Mn_3O_4 and core/shell-structured Rh/Cr_2O_3 as oxygen evolution cocatalyst and hydrogen evolution cocatalysts respectively, resulting in efficient water splitting under visible light [83]. RuO_2, IrO_2, and CoO_x are also possible oxygen evolution cocatalyst candidates, except for Mn_3O_4 [84–93]. Furthermore, the dual cocatalyst strategy could be combined with the facet separation strategy to further improve the POWS efficiency. Takata et al. [24] demonstrated that the efficiency of H_2 and O_2 evolution reactions could be improved separately by selectively photo depositing the cocatalysts Rh/Cr_2O_3 (hydrogen evolution reaction) and CoOOH (oxygen evolution reactions) on different crystal facets of the semiconductor particles $SrTiO_3$:Al (Fig. 6). Overall water splitting of $SrTiO_3$:Al could reach an external quantum efficiency of up to 96% at wavelengths between 350 and 360 nm. This most updated work showed that a suitable photocatalyst design with a simple structure could indeed achieve quantum efficiencies compared with complex protein structures, which would, therefore, promote the advancement of particle photocatalyst for commercial photocatalytic hydrogen production from pure water in the future.

5 Photocatalytic reaction engineering study

The POWS process is a complicated photon-driven physicochemical procedure, coupled with the transfer of light, the adsorption, desorption on interfaces, and the balance of mass and heat in medium. Therefore, in addition to photocatalysts research, photocatalytic reaction engineering study, including reactor design and safety assessment together with establishment of mathematical models to explore the mechanism of photocatalytic reaction engineering, is another crucial part to realize industrial scale-up. It is noted that, although the overall water splitting reaction varies significantly with the half reaction, such reactions share similar photocatalytic reaction engineering principles. Therefore, this part was not limited to the POWS reaction.

Photocatalytic reaction systems can be broadly classified as fixed bed or slurry depending on the form of catalyst. Fixed bed systems attach catalyst particles to the reactor wall or the filling material, which have the advantage of avoiding the need to recover the catalyst. Recently, Nishiyama et al. [6] reported the safe operation of a 100 m^2 panel POWS reactor with a fixed photocatalyst layer containing modified $SrTiO_3$:Al photocatalyst particles (Fig. 7). This system was reported to be capable of

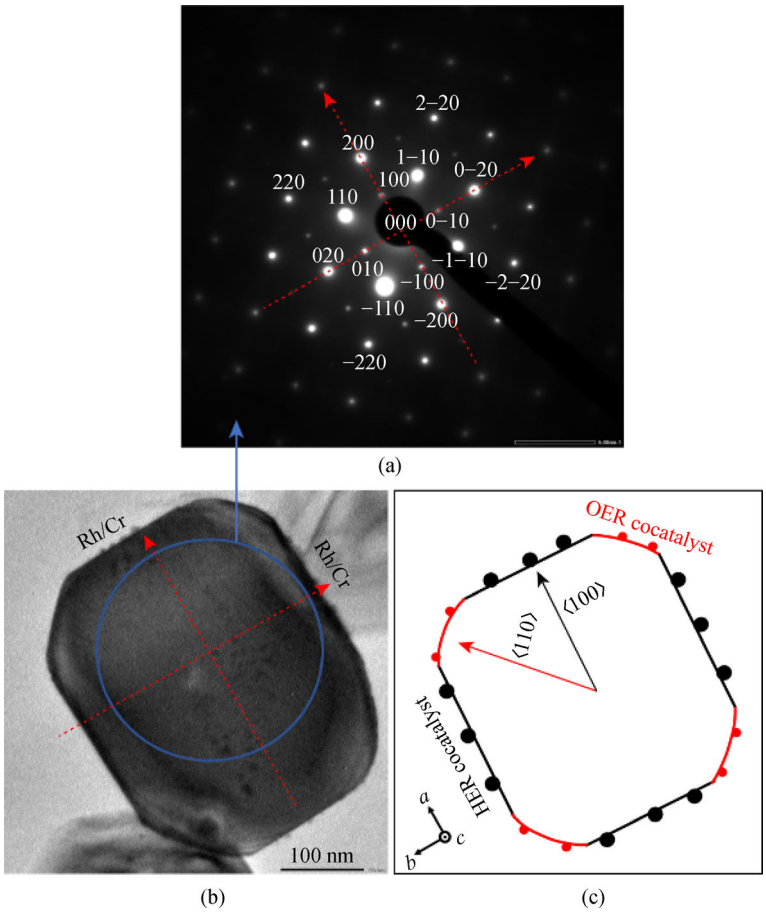

Fig. 6 Structure of Rh /Cr_2O_3 /CoOOH $SrTiO_3$:Al photocatalyst.
(a) Selected-area electron diffraction pattern of Rh /Cr_2O_3 /CoOOH $SrTiO_3$:Al; (b) TEM image of Rh /Cr_2O_3 /CoOOH $SrTiO_3$:Al; (c) morphology of Rh /Cr_2O_3 /CoOOH $SrTiO_3$:Al (adapted with permission from Ref. [24]).

running over several months with autonomous recovery of hydrogen from the gas product mixture. They proved that safe, large-scale photocatalytic water splitting in combination with the key additional functions, i.e., gas collection and separation, is possible.

Slurry systems, on the other hand, disperse catalyst particles directly into the reaction solution and form a suspension by stirring or bubbling, so that the photocatalytic reaction takes place at the interface between the solid particles and the liquid inside the solution. In the slurry system, solid particles and solutions form a multiphase medium containing two or even three solid-liquid-gas phases. In contrast to the homogeneous media, the modeling of photocatalytic reactions in multiphase media must take into account the effects of solid particle light scattering, the solid-liquid two-phase flow, the catalyst concentration distribution, and the reactant adsorption and desorption at the solid-liquid interface in energy and material transport. The compound parabolic concentrator (CPC) coupled photocatalytic hydrogen slurry reactor is a typical slurry reactor (Fig. 8). The CPC is based on the principle of edge optics and is capable of concentrating not only direct light but also obliquely incident sunlight. A photocatalytic reaction system with a CPC concentrator generally consists of the CPC and the reaction tube placed at the bottom of the concentrator, where the incident light passes through the CPC concentrator and shines on the reaction solution in the tube.

Systematic and comprehensive studies of photocatalytic slurry hydrogen production systems using CPC were conducted by Guo et al. [95]. They illustrated that most of the photon energy is lost in the form of light and heat, and only a small fraction can be transferred into hydrogen in the CPC reactor. Moreover, the great differences in time scales between the electron and hole excitation, carrier migration, diffusion and adsorption of reactants and products at the solid-liquid interface and a series of physicochemical processes such as redox reactions and hydrogen nucleation growth involved in this conversion process severely limit the efficiency of photocatalytic hydrogen production. Therefore, it is suggested that the key to developing photocatalytic reaction systems lies in the coupling of multiple physical fields such as light, heat, and reactant flow, overcoming the barriers to energy and

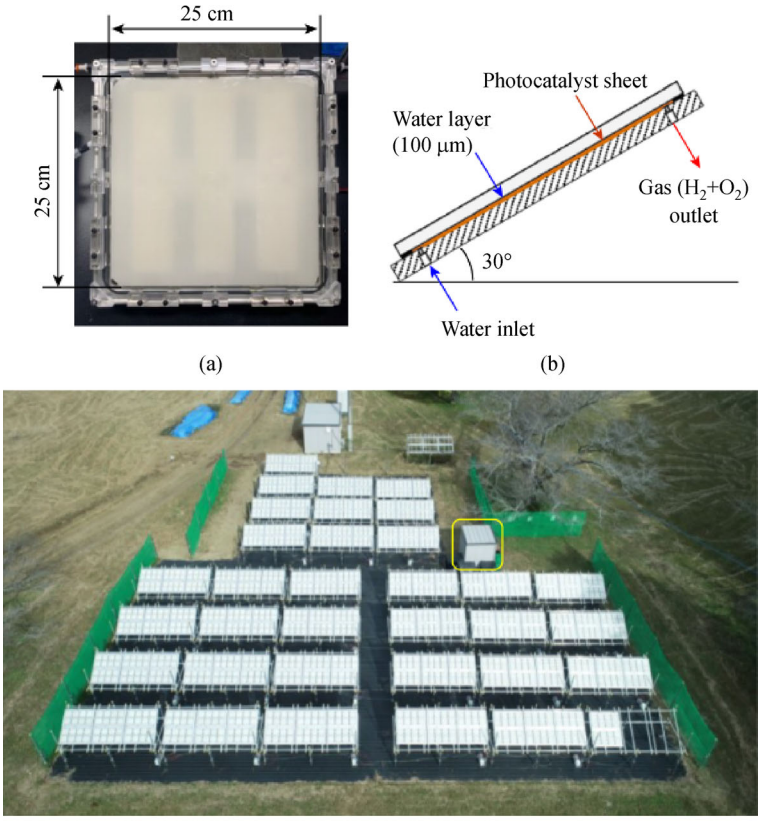

Fig. 7 100 m^2 panel POWS reactor with a fixed photocatalyst layer containing modified $SrTiO_3$:Al photocatalyst particles. (a) A picture of a panel reactor unit; (b) framework of the panel reactor unit system; (c) a view of the 100-m^2 solar POWS system (adapted with permission from Ref. [6]).

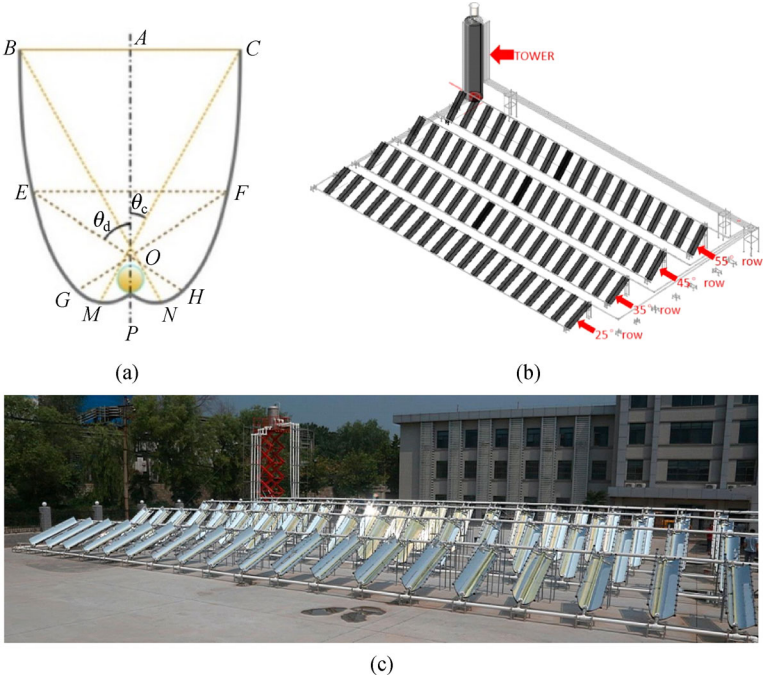

Fig. 8 A compound parabolic concentrator (CPC) coupled photocatalytic hydrogen slurry reactor. (a) Diagrammatic illustration of CPC with a rounded absorber; (b) setup of the designed system; (c) entire CPC-based system for photocatalytic hydrogen production (adapted with permission from Ref. [94]).

material transport, and reducing the time differences in energy and material migration processes, so as to achieve an orderly and efficient conversion of light energy to hydrogen energy.

For example, Ren et al. [96] studied the performance of the tubular reactor in combined with CPC via simulation of distribution of the particle concentration and the radiation inside the reactor and how they combine to effect the radiation absorption. As a conclusion, when the inlet velocity is increased by more than 0.06 m/s and the particle size is controlled below 10 μm, the particulate slurry can be kept well suspended. Moreover, the sluggish flow velocity and large particle size are found to cause specific catalyst concentration gradient which can contribute to the enhancement of radiation absorption within the reactor. Furthermore, the flow properties of the photocatalyst nanoparticle in the reactor were studied by utilizing an experimental setup [97]. It is found that as time increases, the volume fraction of nanoparticle changes and shows a periodical attenuated oscillation. This phenomenon is corresponded to the velocity distribution in the laminar flow, and the period is proportional to the length of the experimental section and inversely proportional to the flow rate. A later research indicates that the continuous working mode of photocatalytic reaction cannot exhibit the highest hydrogen production. There exists an optimal residence and exposure time for photocatalytic reaction fluids that work intermittently. Such phenomenon is ascribed to the balance between efficient use of the solar photon flux and agglomeration and sedimentation of the photocatalyst particles with increased stopping time [98].

In addition to the reaction engineering conditions, the morphology of the photocatalyst could also influence the system performance at the reaction engineering level. Zeng et al. [99] recently showed that a high light intensity resulted in the transform of physical properties of nanosphere TiO_2 (higher thermal conductivity, lower viscosity and the variation of wettability over particle surface) reaction solution and caused severe aggregation, compared with the relative stable performance of nanorod and nanosheet TiO_2. The nanosphere TiO_2 reaction slurry also exhibited a lower temperature than nanorod and nanosheet TiO_2 under the same condition. Therefore, fewer photo-induced charge carriers and slower reaction kinetics resulted in the decreasing hydrogen production at high light intensities over nanosphere TiO_2.

Such photocatalytic reaction engineering study provided useful guidance for targeted reactor design and synthesis of photocatalyst, which is crucial for scale-up photocatalytic water splitting reaction in the future.

6 Future outlook

In 1874, science fiction author Jules Verne set out a prescient vision in his book “The Mysterious Island.” He said “water will one day be employed as fuel, that hydrogen and oxygen which constitute it, used singly or together, will furnish an inexhaustible source of heat and light, of an intensity of which coal is not capable.” This fantasy fiction delivered the human’s belief in the infinite creativity of mankind and the immense power of science. The discovery of Akira Fujishima in 1967 opened a door of hope for mankind in the production of hydrogen by splitting water using photocatalysis [100]. The above review demonstrated that, extensive effort has been made in the past decades to design new photocatalyst materials and systems with an improved overall water splitting efficiency as shown in Fig. 9. We have tried to summarize most of the recent research concerning the POWS recently.

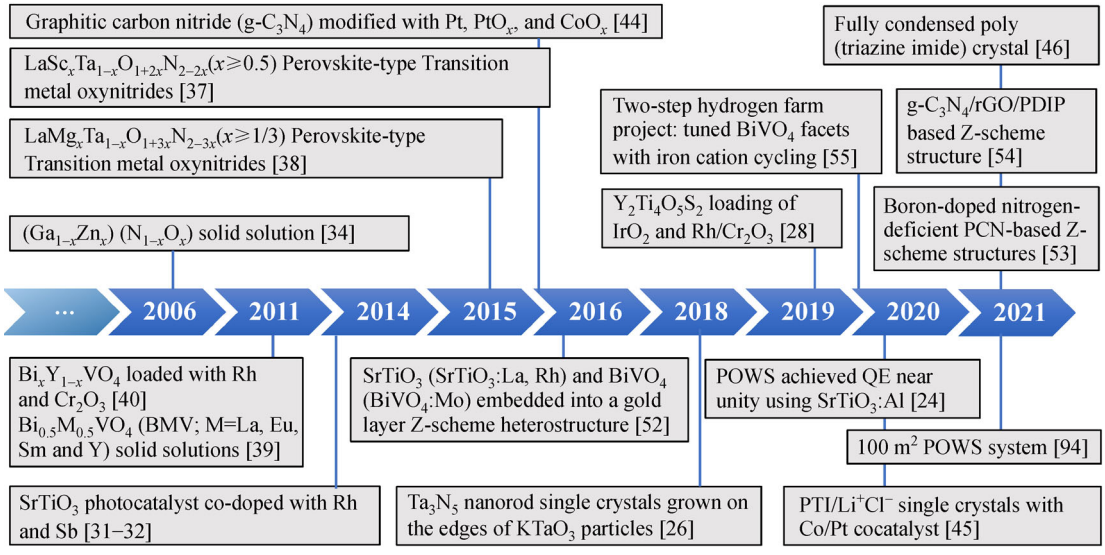

Fig. 9 Recent advance in POWS photocatalyst materials and system.

However, as so many researcher devotes to this area, we note that some significant contributions in this area may still be overlooked due to our vision.

Although the photocatalytic overall water splitting reaction is a tough reaction, using the almost unity quantum efficiency photocatalyst ($SrTiO_3$:Al) as an example, the following conclusion could be reached: Designing photocatalyst with tailored chemistry and physical properties is a successful pathway to greatly improve the overall water splitting activity to reach the commercial goal of solar hydrogen. To achieve the commercial goal of solar energy to hydrogen conversion, having a fundamental understanding of the basic properties of photocatalyst and the reaction engineering in a quantitative manner is of crucial importance in the future design of high efficiency photocatalysts [101]. The challenge on getting more direct mechanism insight lies in the multiple roles of photocatalyst, from photon absorber, interfacial charge transfers to surface catalysis. In the future, under the assistance of the updated spectrum characterization [102–106], improved understanding of the charge transfer dynamics and surface catalysis reaction mechanism could help design smart strategies and further improve the STH efficiency until finally reach the commercial goal.

Acknowledgements This work was supported by the National Natural Science Foundation of China (No. 21872093), the National Key Research and Development Program of China (No. 2018YFB1502001), and the funding support from the Center of Hydrogen Science, Shanghai Jiao Tong University, China.

References

1. Wang Q, Domen K. Particulate photocatalysts for light-driven water splitting: mechanisms, challenges, and design strategies. Chemical Reviews, 2020, 120(2): 919–985
2. Osterloh F E. Photocatalysis versus photosynthesis: a sensitivity analysis of devices for solar energy conversion and chemical transformations. ACS Energy Letters, 2017, 2(2): 445–453
3. Kamat P V, Jin S. Semiconductor photocatalysis: "Tell us the complete story!" ACS Energy Letters, 2018, 3(3): 622–623
4. Chen S, Takata T, Domen K. Particulate photocatalysts for overall water splitting. Nature Reviews Materials, 2017, 2(10): 17050
5. Fabian D M, Hu S, Singh N, et al. Particle suspension reactors and materials for solar-driven water splitting. Energy & Environmental Science, 2015, 8(10): 2825–2850
6. Nishiyama H, Yamada T, Nakabayashi M, et al. Photocatalytic solar hydrogen production from water on a 100 m^2 scale. Nature, 2021, 598(7880): 304–307
7. Kudo A, Kato H, Tsuji I. Strategies for the development of visible-light-driven photocatalysts for water splitting. Chemistry Letters, 2004, 33(12): 1534–1539
8. Hoffmann M R, Martin S T, Choi W, et al. Environmental applications of semiconductor photocatalysis. Chemical Reviews, 1995, 95(1): 69–96
9. Linsebigler A L, Lu G, Yates J T Jr. Photocatalysis on TiO_2 surfaces: principles, mechanisms, and selected results. Chemical Reviews, 1995, 95(3): 735–758
10. Chen X, Shen S, Guo L, et al. Semiconductor-based photocatalytic hydrogen generation. Chemical Reviews, 2010, 110(11): 6503–6570
11. Maeda K, Domen K. Photocatalytic water splitting: recent progress and future challenges. Journal of Physical Chemistry Letters, 2010, 1(18): 2655–2661
12. Leung D Y, Fu X, Wang C, et al. Hydrogen production over titania-Based photocatalysts. ChemSusChem, 2010, 3(6): 681–694
13. Abe R. Recent progress on photocatalytic and photoelectrochemical water splitting under visible light irradiation. Journal of Photochemistry and Photobiology C, Photochemistry Reviews, 2010, 11(4): 179–209
14. Yang J, Wang D, Han H, et al. Roles of cocatalysts in photocatalysis and photoelectrocatalysis. Accounts of Chemical Research, 2013, 46(8): 1900–1909
15. Fujishima A, Zhang X, Tryk D A. TiO_2 photocatalysis and related surface phenomena. Surface Science Reports, 2008, 63(12): 515–582
16. Ni M, Leung M K H, Leung D Y C, et al. A review and recent developments in photocatalytic water-splitting using TiO_2 for hydrogen production. Renewable & Sustainable Energy Reviews, 2007, 11(3): 401–425
17. Kudo A. Photocatalyst materials for water splitting. Catalysis Surveys from Asia, 2003, 7(1): 31–38
18. Maeda K. Photocatalytic water splitting using semiconductor particles: history and recent developments. Journal of Photochemistry and Photobiology C, Photochemistry Reviews, 2011, 12(4): 237–268
19. Serpone N, Emeline A V, Ryabchuk V K, et al. Why do hydrogen and oxygen yields from semiconductor-based photocatalyzed water splitting remain disappointingly low? Intrinsic and extrinsic factors impacting surface redox reactions. ACS Energy Letters, 2016, 1(5): 931–948
20. Gong J, Li C, Wasielewski M R. Advances in solar energy conversion. Chemical Society Reviews, 2019, 48(7): 1862–1864
21. Yamaguchi Y, Kudo A. Visible light responsive photocatalysts developed by substitution with metal cations aiming at artificial photosynthesis. Frontiers in Energy, 2021, 15(3): 568–576
22. Shangguan W, Kudo A, Jiang Z, et al. Photocatalysis: from solar light to hydrogen energy. Frontiers in Energy, 2021, 15(3): 565–567
23. Kudo A, Miseki Y. Heterogeneous photocatalyst materials for water splitting. Chemical Society Reviews, 2009, 38(1): 253–278
24. Takata T, Jiang J, Sakata Y, et al. Photocatalytic water splitting with a quantum efficiency of almost unity. Nature, 2020, 581 (7809): 411–414
25. Asahi R, Morikawa T, Ohwaki T, et al. Visible-light photocatalysis in nitrogen-doped titanium oxides. Science, 2001, 293(5528): 269–271
26. Wang Z, Inoue Y, Hisatomi T, et al. Overall water splitting by Ta_3N_5 nanorod single crystals grown on the edges of $KTaO_3$ particles. Nature Catalysis, 2018, 1(10): 756–763

27. Wolff C M, Frischmann P D, Schulze M, et al. All-in-one visible-light-driven water splitting by combining nanoparticulate and molecular co-catalysts on CdS nanorods. Nature Energy, 2018, 3 (10): 862–869
28. Wang Q, Nakabayashi M, Hisatomi T, et al. Oxysulfide photocatalyst for visible-light-driven overall water splitting. Nature Materials, 2019, 18(8): 827–832
29. Kawasaki S, Akagi K, Nakatsuji K, et al. Elucidation of Rh-induced in-gap states of Rh:$SrTiO_3$ visible-light-driven photocatalyst by soft X-ray spectroscopy and first-principles calculations. Journal of Physical Chemistry C, 2012, 116(46): 24445–24448
30. Konta R, Ishii T, Kato H, et al. Photocatalytic activities of noble metal ion doped $SrTiO_3$ under visible light irradiation. Journal of Physical Chemistry B, 2004, 108(26): 8992–8995
31. Asai R, Nemoto H, Jia Q, et al. A visible light responsive rhodium and antimony-codoped $SrTiO_3$ powdered photocatalyst loaded with an IrO_2 cocatalyst for solar water splitting. Chemical Communications, 2014, 50(19): 2543–2546
32. Niishiro R, Tanaka S, Kudo A. Hydrothermal-synthesized $SrTiO_3$ photocatalyst codoped with rhodium and antimony with visible-light response for sacrificial H_2 and O_2 evolution and application to overall water splitting. Applied Catalysis B: Environmental, 2014, 150–151: 187–196
33. Furuhashi K, Jia Q, Kudo A, et al. Time-resolved infrared absorption study of $SrTiO_3$ photocatalysts codoped with rhodium and antimony. Journal of Physical Chemistry C, 2013, 117(37): 19101–19106
34. Maeda K, Teramura K, Lu D, et al. Photocatalyst releasing hydrogen from water. Nature, 2006, 440(7082): 295
35. Maeda K, Takata T, Hara M, et al. GaN:ZnO solid solution as a photocatalyst for visible-light-driven overall water splitting. Journal of the American Chemical Society, 2005, 127(23): 8286–8287
36. Maeda K, Teramura K, Domen K. Effect of post-calcination on photocatalytic activity of $(Ga_{1-x}Zn_x)(N_{1-x}O_x)$ solid solution for overall water splitting under visible light. Journal of Catalysis, 2008, 254(2): 198–204
37. Pan C, Takata T, Kumamoto K, et al. Band engineering of perovskite-type transition metal oxynitrides for photocatalytic overall water splitting. Journal of Materials Chemistry A, Materials for Energy and Sustainability, 2016, 4(12): 4544–4552
38. Pan C, Takata T, Nakabayashi M, et al. A complex perovskite-type oxynitride: the first photocatalyst for water splitting operable at up to 600 nm. Angewandte Chemie International Edition, 2015, 54 (10): 2955–2959
39. Liu H, Yuan J, Jiang Z, et al. Roles of Bi, M and VO_4 tetrahedron in photocatalytic properties of novel $Bi_{0.5}M_{0.5}VO_4$ (M = La, Eu, Sm and Y) solid solutions for overall water splitting. Journal of Solid State Chemistry, 2012, 186: 70–75
40. Liu H, Yuan J, Jiang Z, et al. Novel photocatalyst of V-based solid solutions for overall water splitting. Journal of Materials Chemistry, 2011, 21(41): 16535–16543
41. Li R, Zhang F, Wang D, et al. Spatial separation of photogenerated electrons and holes among {010} and {110} crystal facets of $BiVO_4$. Nature Communications, 2013, 4(1): 1432
42. Fang W, Jiang Z, Yu L, et al. Novel dodecahedron $BiVO_4$:YVO_4 solid solution with enhanced charge separation on adjacent exposed facets for highly efficient overall water splitting. Journal of Catalysis, 2017, 352: 155–159
43. Wang X, Maeda K, Thomas A, et al. A metal-free polymeric photocatalyst for hydrogen production from water under visible light. Nature Materials, 2009, 8(1): 76–80
44. Zhang G, Lan Z A, Lin L, et al. Overall water splitting by Pt/g-C_3N_4 photocatalysts without using sacrificial agents. Chemical Science (Cambridge), 2016, 7(5): 3062–3066
45. Lin L, Lin Z, Zhang J, et al. Molecular-level insights on the reactive facet of carbon nitride single crystals photocatalysing overall water splitting. Nature Catalysis, 2020, 3(8): 649–655
46. Liu M, Wei C, Zhuzhang H, et al. Fully condensed poly (Triazine Imide) crystals: extended π-conjugation and structural defects for overall water splitting. Angewandte Chemie International Edition, 2021, 61: e20211338
47. Xiao J D, Jiang H L. Metal–organic frameworks for photocatalysis and photothermal catalysis. Accounts of Chemical Research, 2019, 52(2): 356–366
48. Yang Q, Luo M, Liu K, et al. Covalent organic frameworks for photocatalytic applications. Applied Catalysis B: Environmental, 2020, 276(5): 119174
49. Lu R, Liu C, Chen Y, et al. Effect of linkages on photocatalytic H_2 evolution over covalent organic frameworks. Journal of Photochemistry and Photobiology A, Chemistry, 2021, 421(1): 113546
50. Zhang S, Cheng G, Guo L, et al. Strong-base-assisted synthesis of a crystalline covalent triazine framework with high hydrophilicity via benzylamine monomer for photocatalytic water splitting. Angewandte Chemie International Edition, 2020, 59(15): 6007–6014
51. Wang Y, Suzuki H, Xie J, et al. Mimicking natural photosynthesis: Solar to renewable H_2 fuel synthesis by Z-Scheme water splitting systems. Chemical Reviews, 2018, 118(10): 5201–5241
52. Wang Q, Hisatomi T, Jia Q, et al. Scalable water splitting on particulate photocatalyst sheets with a solar-to-hydrogen energy conversion efficiency exceeding 1%. Nature Materials, 2016, 15 (6): 611–615
53. Zhao D, Wang Y, Dong C L, et al. Boron-doped nitrogen-deficient carbon nitride-based Z-scheme heterostructures for photocatalytic overall water splitting. Nature Energy, 2021, 6(4): 388–397
54. Chen X, Wang J, Chai Y, et al. Efficient photocatalytic overall water splitting induced by the giant internal electric field of a g-C_3N_4/rGO/PDIP Z-Scheme heterojunction. Advanced Materials, 2021, 33(7): 2007479
55. Zhao Y, Ding C, Zhu J, et al. A hydrogen farm strategy for scalable solar hydrogen production with particulate photocatalysts. Angewandte Chemie International Edition, 2020, 59(24): 9653–9658
56. Kong L, Jiang Z, Lai H H, et al. Unusual reactivity of visible-light-responsive AgBr–BiOBr heterojunction photocatalysts. Journal of Catalysis, 2012, 293: 116–125
57. Peng T, Li K, Zeng P, et al. Enhanced photocatalytic hydrogen production over graphene oxide–cadmium sulfide nanocomposite under visible light irradiation. Journal of Physical Chemistry C, 2012, 116(43): 22720–22726
58. Negishi Y, Mizuno M, Hirayama M, et al. Enhanced photocatalytic

water splitting by $BaLa_4Ti_4O_{15}$ loaded with ~1 nm gold nanoclusters using glutathione-protected Au25 clusters. Nanoscale, 2013, 5(16): 7188–7192
59. Baba R, Nakabayashi S, Fujishima A, et al. Investigation of the mechanism of hydrogen evolution during photocatalytic water decomposition on metal-loaded semiconductor powders. Journal of Physical Chemistry, 1985, 89(10): 1902–1905
60. Bard A J. Photoelectrochemistry. Science, 1980, 207(4427): 139–144
61. Eastman D. Photoelectric work functions of transition, rare-earth, and noble metals. Physical Review B: Condensed Matter and Materials Physics, 1970, 2(1): 1–2
62. Heller A, Aharon-Shalom E, Bonner W A, et al. Hydrogen-evolving semiconductor photocathodes: nature of the junction and function of the platinum group metal catalyst. Journal of the American Chemical Society, 1982, 104(25): 6942–6948
63. Dai W, Wang X, Liu P, et al. Effects of electron transfer between TiO_2 films and conducting substrates on the photocatalytic oxidation of organic pollutants. Journal of Physical Chemistry B, 2006, 110(27): 13470–13476
64. Jiang Z, Zhang Z, Shangguan W, et al. Photodeposition as a facile route to tunable Pt photocatalysts for hydrogen production: on the role of methanol. Catalysis Science & Technology, 2016, 6(1): 81–88
65. Ikeda T, Xiong A, Yoshinaga T, et al. Polyol synthesis of size-controlled Rh nanoparticles and their application to photocatalytic overall water splitting under visible light. Journal of Physical Chemistry C, 2013, 117(6): 2467–2473
66. Jiang Z, Guo H, Jiang Z, et al. *In situ* controllable synthesis platinum nanocrystals on TiO_2 by novel polyol-process combined with light induced photocatalysis oxidation. Chemical Communications (Cambridge), 2012, 48(77): 9598–9600
67. Jiang Z, Shangguan W. Rational removal of stabilizer-ligands from platinum nanoparticles supported on photocatalysts by self-photocatalysis degradation. Catalysis Today, 2015, 242: 372–380
68. Jiang Z, Isaacs M A, Huang Z W, et al. Active site elucidation and optimization in Pt co-catalysts for photocatalytic hydrogen production over Titania. ChemCatChem, 2017, 9(22): 4268–4274
69. Jiang Z, Sun Z, Yang Y, et al. The role of metal oxide interactions: revisiting Pt growth on the TiO_2 surface in the process of impregnation method. Nanoscale, 2017, 9(37): 14272–14279
70. Jiang Z, Guo H, Jiang Z, et al. *In situ* controllable synthesis platinum nanocrystals on TiO_2 by novel polyol-process combined with light induced photocatalysis oxidation. Chemical Communications, 2012, 48(77): 9598–9600
71. Wang Z, Luo Y, Hisatomi T, et al. Sequential cocatalyst decoration on $BaTaO_2N$ towards highly-active Z-scheme water splitting. Nature Communications, 2021, 12(1): 1005
72. Qureshi M, Garcia-Esparza A T, Jeantelot G, et al. Catalytic consequences of ultrafine Pt clusters supported on $SrTiO_3$ for photocatalytic overall water splitting. Journal of Catalysis, 2019, 376: 180–190
73. Domen K, Naito S, Onishi T, et al. Photocatalytic decomposition of water vapour on an NiO-$SrTiO_3$ catalyst. Journal of the Chemical Physical Letters, 1982, 92(4): 443–544
74. Domen K, Naito S, Onishi T, et al. Study of the photocatalytic decomposition of water vapor over a nickel (II) oxide-strontium titanate ($SrTiO_3$) catalyst. Journal of Physical Chemistry, 1982, 86 (18): 3657–3661
75. Maeda K, Teramura K, Lu D, et al. Noble-metal/Cr_2O_3 core/shell nanoparticles as a cocatalyst for photocatalytic overall water splitting. Angewandte Chemie, 2006, 118(46): 7970–7973
76. Yoshida M, Takanabe K, Maeda K, et al. Role and function of noble-metal/Cr-layer core/shell structure cocatalysts for photocatalytic overall water splitting studied by model electrodes. Journal of Physical Chemistry C, 2009, 113(23): 10151–10157
77. Takata T, Pan C, Nakabayashi M, et al. Fabrication of a core–shell-type photocatalyst via photodeposition of group IV and V transition metal oxyhydroxides: an effective surface modification method for overall water splitting. Journal of the American Chemical Society, 2015, 137(30): 9627–9634
78. Ning X, Lu G. Photocorrosion inhibition of CdS-based catalysts for photocatalytic overall water splitting. Nanoscale, 2020, 12(3): 1213–1223
79. Ning X, Zhen W, Zhang X, et al. Assembly of ultra-thin NiO layer over $Zn_{1-x}Cd_xS$ for stable visible-light photocatalytic overall water splitting. ChemSusChem, 2019, 12(7): 1410–1420
80. Dong J, Zhang X, Lu G, et al. Generation of enhanced stability of SnO/$In(OH)_3$/InP for photocatalytic water splitting by SnO protection layer. Frontiers in Energy, 2021, 15(3): 710–720
81. Zhang X, Lu G, Wu Y, et al. TiO_2 protection layer and well-matched interfaces enhance the stability of Cu_2ZnSnS_4/CdS/TiO_2 for visible light driven water splitting. Catalysis Science & Technology, 2021, 11(16): 5505–5517
82. Ning X, Zhen W, Wu Y, et al. Inhibition of CdS photocorrosion by Al_2O_3 shell for highly stable photocatalytic overall water splitting under visible light irradiation. Applied Catalysis B: Environmental, 2018, 226: 373–383
83. Maeda K, Xiong A, Yoshinaga T, et al. Photocatalytic overall water splitting promoted by two different cocatalysts for hydrogen and oxygen evolution under visible light. Angewandte Chemie International Edition, 2010, 49(24): 4096–4099
84. Sato J, Saito N, Yamada Y, et al. RuO_2-loaded β-Ge_3N_4 as a non-oxide photocatalyst for overall water splitting. Journal of the American Chemical Society, 2005, 127(12): 4150–4151
85. Maeda K, Abe R, Domen K. Role and function of ruthenium species as promoters with TaON-based photocatalysts for oxygen evolution in two-step water splitting under visible light. Journal of Physical Chemistry C, 2011, 115(7): 3057–3064
86. Wang D, Hisatomi T, Takata T, et al. Core/shell photocatalyst with spatially separated co-catalysts for efficient reduction and oxidation of water. Angewandte Chemie International Edition, 2013, 52 (43): 11252–11256
87. Meekins B H, Kamat P V. Role of water oxidation catalyst IrO_2 in shuttling photogenerated holes across TiO_2 interface. Journal of Physical Chemistry Letters, 2011, 2(18): 2304–2310
88. Youngblood W J, Lee S H A, Kobayashi Y, et al. Photoassisted overall water splitting in a visible light-absorbing dye-sensitized photoelectrochemical cell. Journal of the American Chemical Society, 2009, 131(3): 926–927
89. Ma B, Yang J, Han H, et al. Enhancement of photocatalytic water oxidation activity on $IrO_x-ZnO/Zn_{2-x}GeO_{4-x-3y}N_{2y}$ catalyst

with the solid solution phase junction. Journal of Physical Chemistry C, 2010, 114(29): 12818–12822

90. Iwase A, Kato H, Kudo A. A novel photodeposition method in the presence of nitrate ions for loading of an iridium oxide cocatalyst for water splitting. Chemistry Letters, 2005, 34(7): 946–947
91. Ma S S K, Hisatomi T, Maeda K, et al. Enhanced water oxidation on Ta_3N_5 photocatalysts by modification with alkaline metal salts. Journal of the American Chemical Society, 2012, 134(49): 19993–19996
92. Zhang F, Yamakata A, Maeda K, et al. Cobalt-modified porous single-crystalline $LaTiO_2N$ for highly efficient water oxidation under visible light. Journal of the American Chemical Society, 2012, 134(20): 8348–8351
93. Li R, Chen Z, Zhao W, et al. Sulfurization-assisted cobalt deposition on $Sm_2Ti_2S_2O_5$ photocatalyst for water oxidation under visible light irradiation. Journal of Physical Chemistry C, 2013, 117(1): 376–382
94. Wei Q, Yang Y, Hou J, et al. Direct solar photocatalytic hydrogen generation with CPC photoreactors: system development. Solar Energy, 2017, 153: 215–223
95. Guo L, Chen Y, Su J, et al. Obstacles of solar-powered photocatalytic water splitting for hydrogen production: a perspective from energy flow and mass flow. Energy, 2019, 172: 1079–1086
96. Ren Y, Zhao L, Jing D, et al. Investigation and modeling of CPC based tubular photocatalytic reactor for scaled-up hydrogen production. International Journal of Hydrogen Energy, 2016, 41 (36): 16019–16031
97. Geng J, Tang J, Wang Y, et al. Attenuated periodical oscillation characteristics in a nanoscale particle-laden laminar flow. Industrial & Engineering Chemistry Research, 2020, 59(16): 8018–8027
98. Zeng Z, Sun L, Liu H, et al. Should the tubular photocatalytic reactors work continuously or in an intermittent manner instead? Industrial & Engineering Chemistry Research, 2021, 60(12): 4610–4621
99. Zeng Z, Luo B, Jing D, et al. Hydrogen production versus photocatalyst dimension under concentrated solar light: a case over titanium dioxide. Solar Energy, 2021, 230: 538–548
100. Fujishima A, Honda K. Electrochemical photolysis of water at a semiconductor electrode. Nature, 1972, 238(5358): 37–38
101. Takanabe K. Photocatalytic water splitting: quantitative approaches toward photocatalyst by design. ACS Catalysis, 2017, 7(11): 8006–8022
102. Tang J, Durrant J R, Klug D R. Mechanism of photocatalytic water splitting in TiO_2. Reaction of water with photoholes, importance of charge carrier dynamics, and evidence for four-hole chemistry. Journal of the American Chemical Society, 2008, 130(42): 13885–13891
103. Chen R, Pang S, An H, et al. Charge separation via asymmetric illumination in photocatalytic Cu_2O particles. Nature Energy, 2018, 3(8): 655–663
104. Vinogradov I, Singh S, Lyle H, et al. Free energy difference to create the M-OH* intermediate of the oxygen evolution reaction by time-resolved optical spectroscopy. Nature Materials, 2022, 21(1): 88–94
105. Zhao J, Osterloh F E. Photochemical charge separation in nanocrystal photocatalyst films: insights from surface photovoltage spectroscopy. Journal of Physical Chemistry Letters, 2014, 5(5): 782–786
106. Qi R, Yu P, Zhang J, et al. Efficient visible light photocatalysis enabled by the interaction between dual cooperative defect sites. Applied Catalysis B: Environmental, 2020, 274: 119099